Nano Research 2017, 10(2): 405–414
DOI 10.1007/s12274-016-1334-0
Research Article
ISSN 1998-0124
CN 11-5974/O4

Facile one-pot synthesis of $NiCo_2O_4$ hollow spheres with controllable number of shells for high-performance supercapacitors

Jing Guo, Zhihui Yin, Xiaoxian Zang, Ziyang Dai, Yizhou Zhang, Wei Huang (✉), and Xiaochen Dong (✉)

Key Laboratory of Flexible Electronics (KLOFE) & Institute of Advanced Materials (IAM), Jiangsu National Synergetic Innovation Center for Advanced Materials (SICAM), Nanjing Tech University (NanjingTech), 30 South Puzhu Road, Nanjing 211816, China

Received: 14 August 2016
Revised: 26 September 2016
Accepted: 14 October 2016

KEYWORDS
$NiCo_2O_4$,
hollow spheres,
controlled number of shells,
supercapacitor

ABSTRACT

In this work, single- and double-shelled $NiCo_2O_4$ hollow spheres have been synthesized *in situ* by a one-pot solvothermal method assisted by xylose, followed by heat treatment. Employed as supercapacitor electrode materials, the double-shelled $NiCo_2O_4$ hollow spheres exhibit a remarkable specific capacitance (1,204.4 $F \cdot g^{-1}$ at a current density of 2.0 $A \cdot g^{-1}$) and excellent cycling stability (103.6% retention after 10,000 cycles at a current density of 10 $A \cdot g^{-1}$). Such outstanding electrochemical performance can be attributed to their unique internal morphology, which provides a higher surface area with a larger number of active sites available to interact with the electrolyte. The versatility of this method was demonstrated by applying it to other binary metal oxide materials, such as $ZnCo_2O_4$, $ZnMn_2O_4$, and $CoMn_2O_4$. The present study thus illustrates a simple and general strategy for the preparation of binary transition metal oxide hollow spheres with a controllable number of shells. This approach shows great promise for the development of next-generation high-performance electrochemical materials.

1 Introduction

The ever-growing global energy consumption and the increasing environmental pollution stimulate the exploration of new electrode materials able to meet the requirements of renewable energy devices. Hollow structured nanomaterials with controlled composition, number of shells, and structural complexity have received significant interest during the past few years due to their potential application in various areas, such as photocatalysis [1, 2], gas sensors [3], drug delivery [4–6], water treatment [7], and energy storage [8–12]. The superior structural features of these materials have triggered substantial efforts to design and fabricate hollow materials with well-defined internal morphology, focused in particular on multi-shelled nanostructures, which have shown interesting electrochemical properties in different applications

Address correspondence to Xiaochen Dong, iamxcdong@njtech.edu.cn; Wei Huang, iamwhuang@njtech.edu.cn

[13–15]. To date, multi-shelled nanostructures have been prepared mainly via templating approaches using different hard templates, including monodisperse polymers, metal oxides, and carbonaceous spheres [16, 17]. For example, Yao et al. successfully prepared multi-shelled hollow spheres by using polystyrene divinyl benzene spheres as a sacrificial template, which enhanced the photocatalytic activity [18]. Shi et al. prepared multifunctional hollow-structured nanocapsules using magnetic Fe_3O_4 as a template [19]. Wang et al. synthesized multi-shelled ZnO hollow structures via a temperature-programmed heating treatment using carbonaceous spheres as a template; these spheres exhibited excellent performance in dye-sensitized solar cells [20]. Despite the significant progress made so far, most of the available methods are based on hard templates prepared in advance, which results in a quite tedious procedure, also difficult to apply in mass production [21, 22]. Moreover, these template methods are only suitable for specific materials [23–25], which hinders their further development and practical applications. Therefore, the development of a general method to fabricate hollow structures of mixed metal oxides with a controlled number of shells, preferably through a one-pot process, currently represents a huge challenge.

Binary transition metal oxides (BTMOs) have recently attracted considerable attention in view of their superior redox activity and high natural abundance. Compared to simple transition metal oxides, BTMOs present faster proton transport and multiple achievable oxidation states, as well as fast and reversible faradaic reactivity with ultrahigh specific capacitance [26]. These properties make BTMOs a key class of functional materials. Despite having achieved excellent electrical properties, BTMOs still present limited cycling stability and poor high-rate performance, due to pulverization during charge and discharge processes. Therefore, the design and fabrication of BTMOs with a complex multi-shelled hollow structure represents a crucial task.

Herein, we report a general method to synthesize hollow-structured $NiCo_2O_4$ with controllable number of shells, large specific surface area, significant porosity, and low mass density, via a simple one-pot solvothermal method followed by thermal treatment. The multi-shelled hollow spheres led to high-rate capacitance and remarkable cycling stability when employed as electrode materials for supercapacitors, suggesting that they could represent promising candidates for energy storage applications.

2 Materials and experimental methods

2.1 Synthesis of $NiCo_2O_4$ hollow spheres

All reagents employed in the synthesis were of analytical grade and used without further purification. The products were synthesized by a facile solvothermal method using xylose, $Ni(NO_3)_2{\cdot}6H_2O$, and $Co(NO_3)_2{\cdot}6H_2O$ as raw materials. In a typical experiment, 1.5 mmol xylose, 0.5 mmol $Ni(NO_3)_2{\cdot}6H_2O$, and 1 mmol $Co(NO_3)_2{\cdot}6H_2O$ were added to 30 mL isopropanol (IPA) and stirred for 1 h at room temperature. The mixture was then transferred into a 50 mL Teflon-lined stainless steel autoclave and solvothermally treated at 180 ℃ for 24 h. After naturally cooling down to room temperature, the brown powder was collected by centrifugation and washed several times with deionized (DI) water and ethanol. The single- and double-shelled $NiCo_2O_4$ hollow spheres were generated separately, by heating the precursor to 450 ℃ for 7 h in air with temperature ramping rates of 3 and 5 ℃·min^{-1}, respectively. $NiCo_2O_4$ microspheres were prepared using the same method employed for the double-shelled $NiCo_2O_4$ hollow spheres, but without xylose.

Other metal oxide hollow spheres, such as $ZnCo_2O_4$, $ZnMn_2O_4$, and $CoMn_2O_4$, were also synthesized by this method, using different metal nitrates.

2.2 Materials characterization

X-ray diffraction (XRD, Bruker D8 Advance) was employed to determine the crystallographic structure of the samples. The morphology and internal structure were characterized by field-emission scanning electron microscopy (FESEM, Zeiss Ultra-55) and transmission electron microscopy (TEM, Hitachi, HT7700 and JEOL, 2010), respectively. X-ray photoelectron (XPS) spectra were recorded on a UlVAC-PHI Inc PHI 5000 Versa probe spectrometer from a monochromated Al anode X-ray source with Kα radiation (1,486.6 eV). Thermogravimetric analysis (TGA) was performed with a Shimadzu TGA-50 instrument from room tem-

perature to 600 ℃ at a heating rate of 5 ℃·min^{-1} in air. The surface area of the products was determined by Brunauer–Emmett–Teller (BET) nitrogen adsorption–desorption and Barrett–Joyner–Halenda (BJH) methods (Micromeritics, ASAP2020).

2.3 Electrochemical measurements

All electrochemical measurements were performed on an electrochemical workstation (CHI 660E, CH instrument Inc., China) with a standard three-electrode configuration, with platinum wire and saturated silver/silver chloride (Ag/AgCl) as the counter and reference electrode, respectively. A 6 M KOH solution was used as electrolyte in all measurements. The working electrode was prepared by coating Ni foam with the active materials, acetylene black, and polyvinylidene fluoride (PVDF) binder in 8:1:1 weight ratio. The mass loading of the active material was 2 mg·cm^{-2}. Cyclic voltammetry (CV) measurements were performed in a potential window ranged from −0.1 to 0.55 V vs. saturated calomel electrode (SCE), and galvanostatic charge–discharge (GCD) tests were conducted at different current densities. Electric impedance spectroscopy (EIS) experiments were carried out in a frequency range from 10 mHz to 100 kHz at open circuit potential, by applying an AC voltage with 10 mV amplitude. The following equation was used for calculating the specific capacitance [27]

$$C = I\cdot\Delta t/(m\cdot\Delta V) \quad (1)$$

where C (F·g^{-1}) represents the specific capacitance of the electrode, I (A) is the discharge current, Δt (s) denotes the discharge time, m (g) is the mass loading of the active materials, and ΔV represents the potential window.

3 Results and discussion

The formation of the single- and multi-shelled $NiCo_2O_4$ hollow spheres is schematically illustrated in Fig. 1. In the initial stages of the reaction, condensation and polymerization of xylose lead to the formation of primary carbonaceous spheres under solvothermal conditions. Owing to the presence of large amounts of –OH and C=O functional groups on the external and inner surfaces of the pore channels (Fig. S1 in the Electronic Supplementary Material (ESM)), the significant amount of Ni^{2+} and Co^{2+} ions in solution can be adsorbed by the carbon spheres through electrostatic attraction. Calcination is likely to result in the redistribution of Ni^{2+} and Co^{2+} species over the whole volume of the carbon spheres. When heating is carried out at a slow rate, there is sufficient time for the Ni^{2+} and Co^{2+} ions trapped within the carbon spheres to form a nickel cobaltite thick shell before the carbon spheres shrink and split from the outer functional layer [28]. When the heating rate increases, the spreading of the Ni^{2+} and Co^{2+} ions throughout the whole volume of the carbon spheres is enhanced, leading to deeper penetration of the metal species and finally to the formation of a greater number of shells [24]. Therefore, the multi-shelled hollow spheres are obtained by employing the carbonaceous spheres as sacrificial templates. Remarkably, compared with $NiCo_2O_4$ microspheres, the single- and double-shelled $NiCo_2O_4$ hollow spheres exhibit excellent electrochemical activity.

The as-prepared samples before and after calcination were characterized by XRD (Fig. 2). Only a broad and low-density diffraction peak was detected in the XRD pattern of the precursor, confirming the amorphous nature of the carbonaceous composition [29]. After the heating treatment, the nanocomposites prepared under different experimental conditions present similar

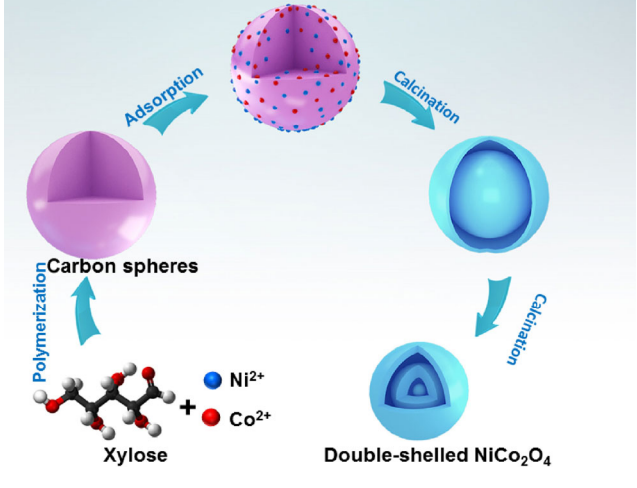

Figure 1 Schematic illustration of the formation of double-shelled $NiCo_2O_4$ hollow spheres.

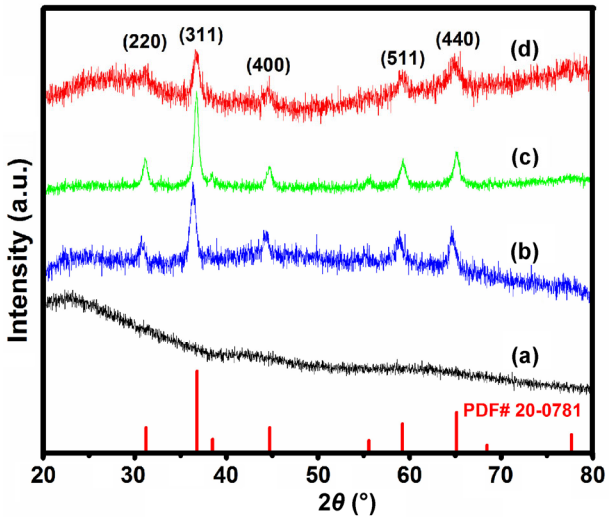

Figure 2 XRD patterns of (a) the precursor of double-shelled $NiCo_2O_4$ hollow spheres, (b) single-shelled and (c) double-shelled $NiCo_2O_4$ hollow spheres, and (d) $NiCo_2O_4$ microspheres.

XRD patterns. All sharp diffraction peaks observed are consistent with the standard diffraction data of face-centered cubic $NiCo_2O_4$ (JCPDS 20-0781), indicating that the products were successfully converted to $NiCo_2O_4$ with good crystallinity. It is worth noting that the wide peak of carbon, formed by condensation and polymerization of xylose, could not be observed in the XRD pattern, suggesting that carbon was entirely removed after calcination in air.

FESEM was employed to explore the morphology of the precursors. As shown in Fig. 3(a), a large amount of microspheres with a relatively smooth surface and distribution are obtained after the solvothermal reaction. The diameter of the microspheres is around 900 nm, much smaller than that of the precursors of the $NiCo_2O_4$ microspheres (Fig. S2 in the ESM). The TEM image in Fig. 3(b) further confirms the fully solid nature of the precursor microspheres. XPS measurements were carried out to analyze the surface composition and oxidation states of the elements present. The two major Ni^{2+} ions peaks are located at 873.5 and 855.8 eV in Fig. 3(c), indicating that Ni^{2+} ions are adsorbed by the carbonaceous precursor spheres during the solvothermal process. Furthermore, Co^{2+} ions undergo the same process as Ni^{2+} ions, as shown in Fig. 3(d). It is worth noting that some Ni^{2+} and Co^{2+} transform into Ni^{3+} and Co^{3+}, respectively, in the subsequent thermal process, as shown by the XPS analysis of the final product (Fig. 5).

After the heating treatment, the precursor is transformed into $NiCo_2O_4$ and the morphology of the microspheres is retained without any severe cracking, as shown in Fig. 4(a). Moreover, the surface of the

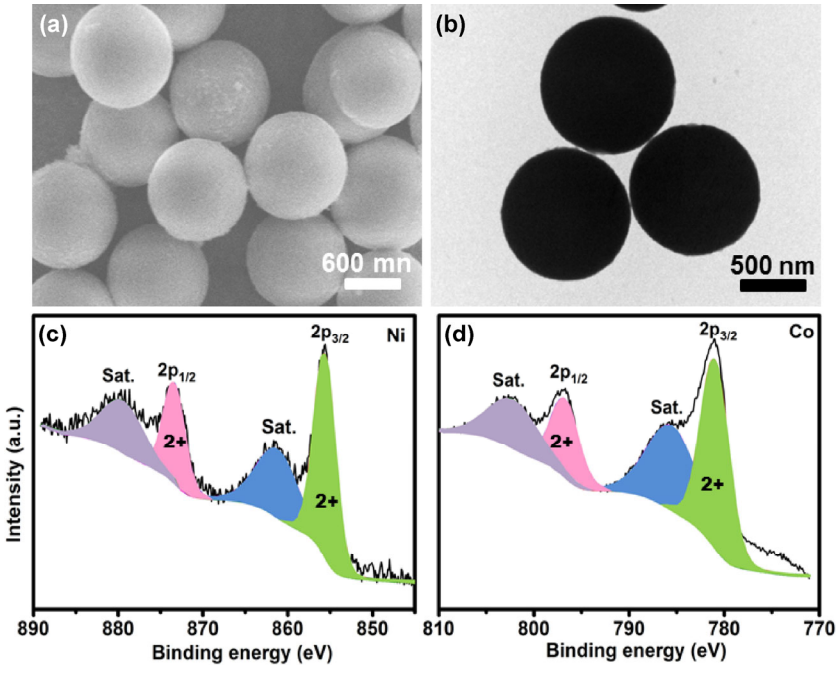

Figure 3 (a) and (b) SEM and TEM images of the precursors of $NiCo_2O_4$ hollow spheres at different magnifications. (c) and (d) Ni 2p and Co 2p of the precursors of $NiCo_2O_4$ hollow spheres.

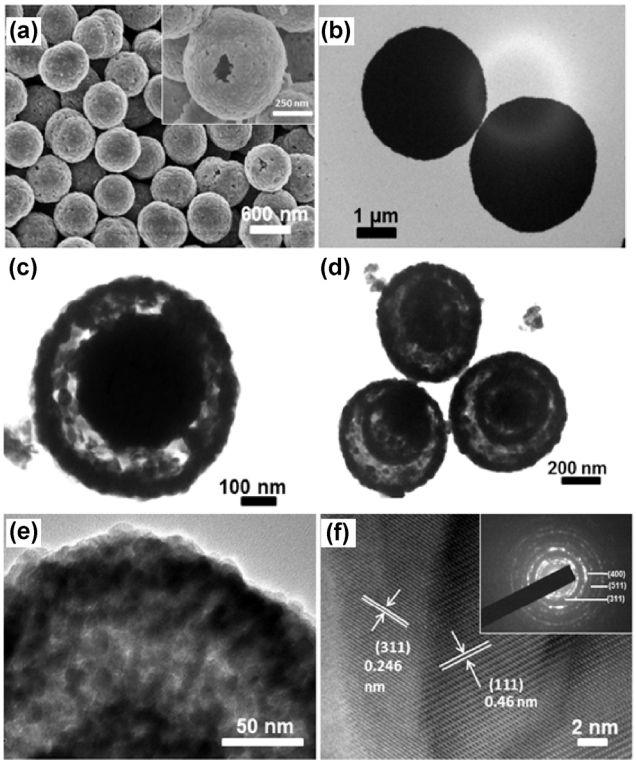

Figure 4 (a) SEM image of double-shelled $NiCo_2O_4$ hollow spheres. The inset shows the magnified SEM image. (b)–(d) TEM images of $NiCo_2O_4$ microspheres and of single- and double-shelled $NiCo_2O_4$ hollow spheres. (e) and (f) HRTEM image and corresponding SAED pattern of double-shelled $NiCo_2O_4$ hollow spheres.

double-shelled $NiCo_2O_4$ microspheres becomes rough with some exposed pores, whose formation is due to the release of CO_2 and H_2O following the structural contraction associated to the thermal decomposition of the precursor (inset of Fig. 4(a)). Further insight into the morphology of the microspheres was obtained from TEM measurements. As shown in Figs. 4(b)–4(d), $NiCo_2O_4$ microspheres as well as single- and double-shelled $NiCo_2O_4$ hollow spheres were obtained after the heating treatment. The different internal morphology indicates that the structure of the hollow spheres is strongly influenced by the heating rate and composition of the precursors. Furthermore, the magnified TEM image (Fig. 4(e)) shows that the shells of the hollow spheres are highly crystalline and composed of small microspheres with an average size around 15 nm. The high resolution TEM (HRTEM) image in Fig. 4(f) displays distinct lattice fringes with *d*-spacing of 0.246 and 0.46 nm, which correspond to the (311) and (111) crystal facets of $NiCo_2O_4$, respectively. The selected-area electron diffraction (SAED) pattern (inset in Fig. 4(f)) shows that the resulting $NiCo_2O_4$ is polycrystalline in nature and the series of concentric rings observed in the SAED pattern can be assigned to the (400), (511), and (311) planes of $NiCo_2O_4$, consistently with the XRD analysis presented above.

Figure 5 shows the XPS spectra of the double-shelled $NiCo_2O_4$ hollow spheres. The survey spectrum in Fig. 5(a) indicates the presence of Ni, Co, and O in these spheres. By applying a Gaussian fitting method, the Ni 2p emission spectrum was fitted with two spin–orbit doublets (Fig. 5(b)), located at 853.38 and 871.08 eV (corresponding to Ni^{2+}) and at 855.58 and 873.38 eV (corresponding to Ni^{3+}) [30]. The Co 2p emission spectrum (Fig. 5(c)) was split into two spin–orbit doublets characteristic of Co^{2+} and Co^{3+} and two shake-up satellites (identified as "Sat." in the figure). The peaks at binding energies of 796.0 and 780.58 eV can be assigned to Co^{2+}, while other peaks at 779.08 and 794.38 eV can be attributed to Co^{3+} [31]. The high-resolution spectrum of the O 1s region, shown in Fig. 5(d), can be divided into four oxygen contributions, labeled O_1, O_2, O_3, and O_4. The O_1 component at 529.38 eV can be attributed to a typical metal–oxygen bond [32]. The O_2 component at 530.98 eV is associated with oxygen in OH^- groups, implying that the surface of $NiCo_2O_4$ is hydroxylated. The O_3 component at 531.98 eV corresponds to the large amount of defect sites [33]. Finally, the O_4 component could be attributed to various types of water molecules physically and chemically bonded onto and within the surface [34]. These results indicate that the electron couples of Ni^{3+}/Ni^{2+} and Co^{3+}/Co^{2+} are codependent in $NiCo_2O_4$ hollow spheres. The TGA of the precursor of the $NiCo_2O_4$ hollow spheres revealed a large weight loss of about 60.0% (Fig. S3 in the ESM). The double-shelled $NiCo_2O_4$ sample was characterized through the N_2 sorption measurements at 77 K shown in Fig. S4 in the ESM, highlighting a BET surface area of 48 $m^2 \cdot g^{-1}$ as well as major pores located around 8 nm.

The above results indicate that the heating rate plays a significant role in the formation of shelled hollow structures. Particularly remarkable is the fact that all the obtained products are either single- or double-shelled, and no other hollow structures with a higher number of shells can be synthesized under

the experimental conditions considered. This finding can be ascribed to the difficulty in controlling the nucleation and growth rate of the NiCo-based compounds in the carbon matrices under solvothermal conditions [23].

The versatility of the present method was further demonstrated by fabricating another set of three different mixed metal oxides, such as $ZnCo_2O_4$, $CoMn_2O_4$, and $ZnMn_2O_4$. The corresponding XRD patterns of the samples match the structures of $ZnCo_2O_4$, $ZnMn_2O_4$, and $CoMn_2O_4$ (Figs. 6(a)–6(c)). Furthermore, the samples have spherical morphology, similar to the $NiCo_2O_4$ hollow spheres. The TEM images confirm that double-shelled hollow spheres can be formed for different materials (Figs. 6(d)–6(f)). Such structures offer surface areas large enough to facilitate electrochemical reactions

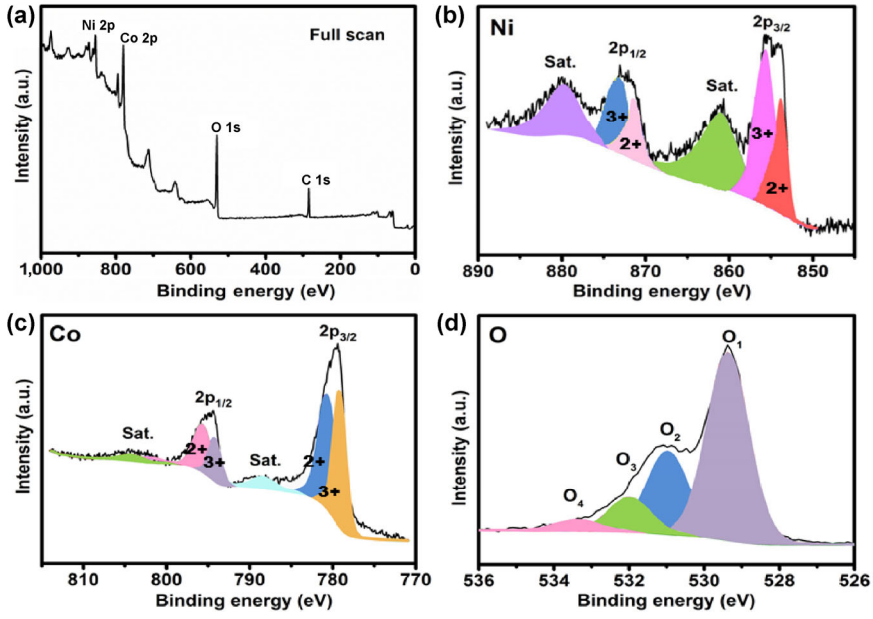

Figure 5 High-resolution XPS spectra of double-shelled $NiCo_2O_4$ hollow spheres. (a) Survey spectrum, (b) Ni 2p spectrum, (c) Co 2p spectrum, and (d) O 1s spectrum.

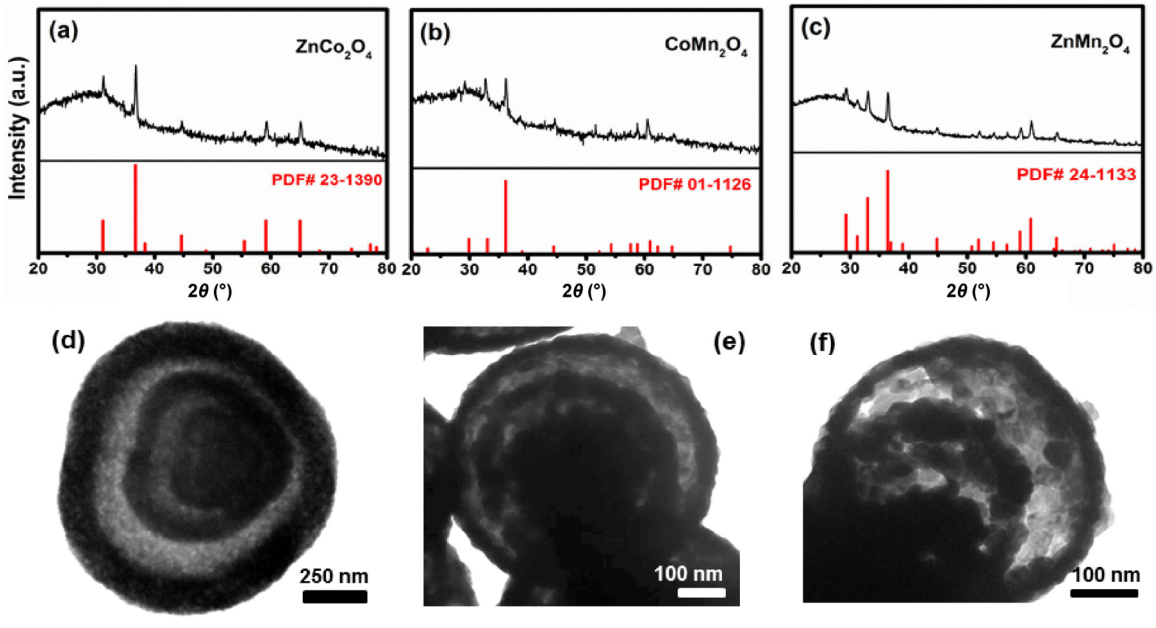

Figure 6 (a)–(c) XRD pattern and (d)–(f) TEM images of $ZnCo_2O_4$, $CoMn_2O_4$, and $ZnMn_2O_4$.

and efficient penetration of the electrolyte into the active materials, leading to excellent electrochemical properties (Fig. S5 in the ESM).

Figure 7(a) shows the typical CV curves of double-shelled $NiCo_2O_4$ spheres at different sweep rates. A pair of distinct peaks can be observed in the potential window from −0.1 to 0.55 V vs. SCE, caused by the faradaic redox reactions of M–O/M–O–OH species (where M stands for Ni or Co). The following redox reactions occur in $NiCo_2O_4$ [35]

$$NiCo_2O_4 + OH^- + H_2O \leftrightarrow NiOOH + 2CoOOH + e^- \quad (2)$$

$$CoOOH + OH^- \leftrightarrow CoO_2 + H_2O + e^- \quad (3)$$

The position of the cathodic peak is slightly shifted towards negative potentials when the sweep rate increases from 0.34 to 0.44 V, due to the rapid diffusion rate of the electrons and ion on the surface of the electrode during the redox reaction [36]. Figure 7(b) shows the GCD curves obtained with current densities ranging from 2 to 40 $A \cdot g^{-1}$. Marked voltage plateaus are apparent in the charge/discharge curves for all current densities, which is a typical characteristic of pseudocapacitive behavior. The specific capacitance of $NiCo_2O_4$ hollow spheres electrodes was calculated from the GCD measurements based on Eq. (1). As shown in Fig. 7(c), the double-shelled $NiCo_2O_4$ hollow sphere electrode yields high capacitances of 1,204.4, 1,108.4, 1,062.6, 1,018.6, 882.2, 822.2, and 702.2 $F \cdot g^{-1}$ at current densities of 2, 4, 6, 8, 10, 20, and 40 $A \cdot g^{-1}$, respectively, which are much higher than the capacitances measured for the other two samples. The double-shelled hollow structure retains 58.3% of its initial specific capacitance even at a current density of 40 $A \cdot g^{-1}$. This value is higher than the capacity retention of the single-shelled hollow structures (49.6%) and of the solid microspheres (56.3%), highlighting the superior retention capability of the double-shelled $NiCo_2O_4$ spheres. To evaluate the long-term cycling stability of the electrode, the GCD test was repeated at a constant current density of 10 $A \cdot g^{-1}$ (Fig. 7(d)). The double-shelled $NiCo_2O_4$ electrode delivers a high capacitance

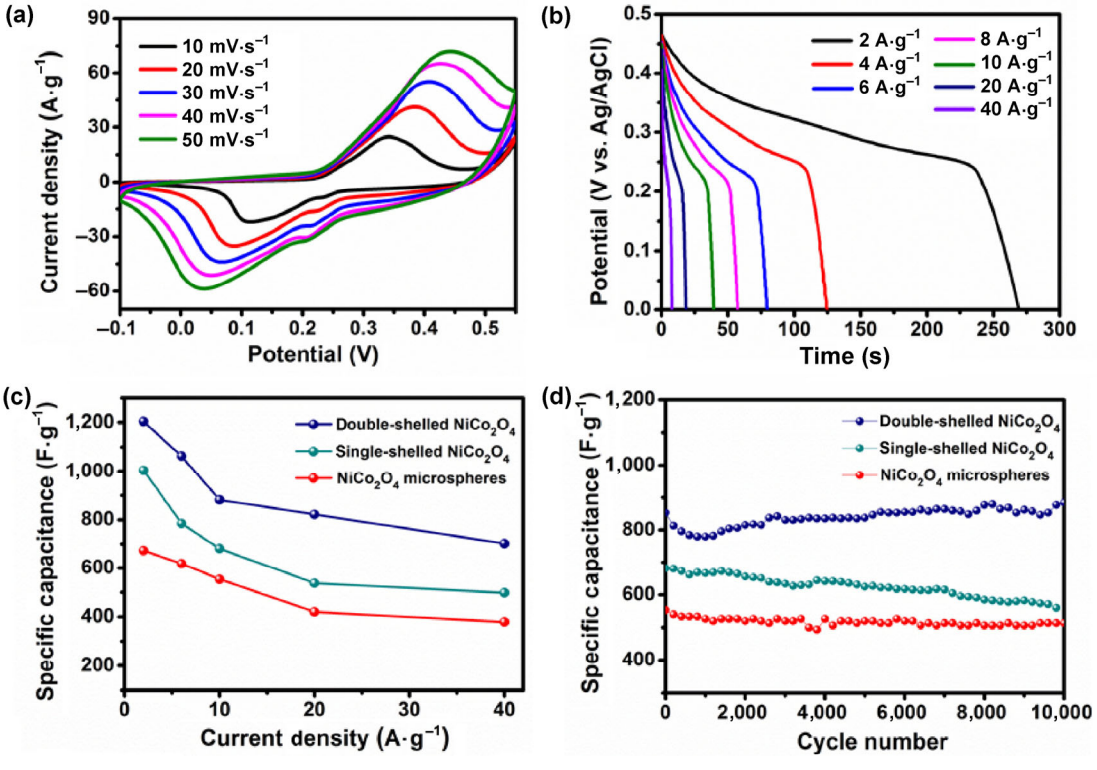

Figure 7 (a) Cyclic voltammograms of double-shelled $NiCo_2O_4$ hollow spheres at different scan rates. (b) GCD curves of double-shelled $NiCo_2O_4$ hollow spheres at various current densities. (c) Specific capacitance of single- and double-shelled $NiCo_2O_4$ hollow spheres and of $NiCo_2O_4$ microspheres at different current densities. (d) Cycling performance of single- and double-shelled $NiCo_2O_4$ hollow spheres and of $NiCo_2O_4$ microspheres at 10 $A \cdot g^{-1}$.

of 882.2 $F \cdot g^{-1}$ and a longer cycling life with 103.6% capacity retention over 10,000 cycles, whereas only 82.2% and 92.7% of the initial capacitance was retained by single-shelled $NiCo_2O_4$ and $NiCo_2O_4$ microspheres, respectively. The double-shelled hollow spheres retained their structure after 10,000 cycles and the $NiCo_2O_4$ structure was stable, without any other impurity formed (Fig. S6 in the ESM). Their superior electrochemical performance can be attributed to the favorable structural characteristics of the unique double-shelled hollow structure and to the high porosity of the $NiCo_2O_4$ hollow spheres. The porous structure provides good ion accessibility and rapid mass transport, which is beneficial to achieve efficient redox reactivity. Moreover, the double-shelled hollow structure can provide a higher amount of active sites and facilitate the transport of the electrolyte, achieving superior high-rate capability compared with the $NiCo_2O_4$ electrodes reported in literature (Table S1 in the ESM).

The enhanced electrochemical performance of $NiCo_2O_4$ spheres with different internal morphology was investigated by EIS measurements in the frequency range from 10^{-2} to 10^5 Hz. The Nyquist plots of the samples displayed in Fig. 8 are composed of a small-diameter semicircle and a steep straight line. The axis intercept in the high-frequency region yields the bulk resistance of the electrochemical system (*R*s) and the high slope of the EIS curve in the low-frequency region indicates a low diffusion resistance. The internal resistances of single- and double-shelled $NiCo_2O_4$ spheres and of $NiCo_2O_4$ microspheres are 0.44, 0.56, and 0.8 Ω, respectively. The slope of the EIS curve for double-shelled $NiCo_2O_4$ spheres is much higher than that of the other two systems examined. These results imply that the double-shelled $NiCo_2O_4$ spheres have a much lower resistance and are more electrochemically active than their counterparts synthesized through different methods.

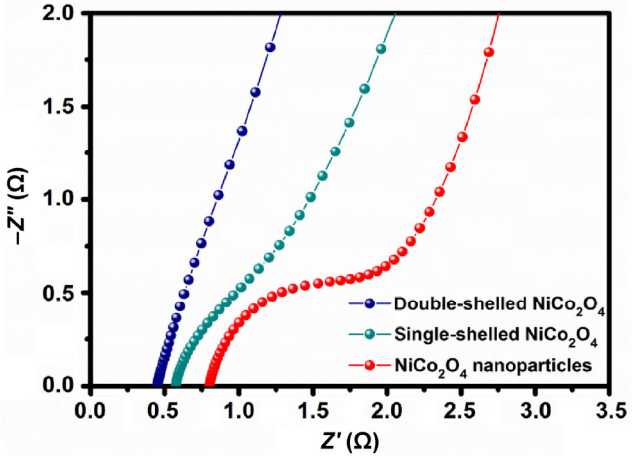

Figure 8 EIS spectrum of electrodes based on single- and double-shelled $NiCo_2O_4$ hollow spheres and on $NiCo_2O_4$ microspheres.

4 Conclusions

A simple, efficient, and versatile strategy to fabricate $NiCo_2O_4$ hollow spheres with a controllable number of shells was demonstrated. The present approach involves a solvothermal synthesis assisted by xylose and subsequent heat treatment. The present experiments demonstrate that the heating rate and composition of the precursors play a key role in the formation of the hollow spheres. The double-shelled $NiCo_2O_4$ hollow spheres exhibit ultrahigh specific capacitance and long cycle life when applied in supercapacitor electrodes. This finding can be attributed to their unique hollow structure, which can accelerate ion/electron transfer and improve the electrochemical performance. The versatility of this method was also demonstrated by applying it to other binary metal oxide materials, such as $ZnCo_2O_4$, $ZnMn_2O_4$, and $CoMn_2O_4$. The present approach to synthesize systems with a controlled number of shells shows great potential for the cost-effective and large-scale production of energy storage materials.

Acknowledgements

The work was supported by the National Natural Science Foundation of China (Nos. 61525402 and 21275076), Key University Science Research Project of Jiangsu Province (No. 15KJA430006), Jiangsu Provincial Founds for Distinguished Young Scholars (No. BK20130046), Program for New Century Excellent Talents in University (No. NCET-13-0853), QingLan Project.

Electronic Supplementary Material: Supplementary material (FTIR spectrum, SEM, TGA, XRD pattern, N_2 adsorption–desorption isothermal, electrochemical

measurements, etc.) is available in the online version of this article at http://dx.doi.org/10.1007/s12274-016-1334-0.

References

[1] Oh, M. H.; Yu, T.; Yu, S.-H.; Lim, B.; Ko, K.-T.; Willinger, M.-G.; Seo, D.-H.; Kim, B. H.; Cho, M. G.; Park, J.-H. et al. Galvanic replacement reactions in metal oxide nanocrystals. *Science* **2013**, *340*, 964–968.

[2] Joo, J. B.; Zhang, Q.; Dahl, M.; Lee, I.; Goebl, J.; Zaera, F.; Yin, Y. D. Control of the nanoscale crystallinity in mesoporous TiO_2 shells for enhanced photocatalytic activity. *Energy Environ. Sci.* **2012**, *5*, 6321–6327.

[3] Lai, X. Y.; Halpert, J. E.; Wang, D. Recent advances in micro-/nano-structured hollow spheres for energy applications: From simple to complex systems. *Energy Environ. Sci.* **2012**, *5*, 5604–5618.

[4] Hyuk Im, S.; Jeong, U.; Xia, Y. N. Polymer hollow particles with controllable holes in their surfaces. *Nat. Mater.* **2005**, *4*, 671–675.

[5] Liu, J.; Qiao, S. Z.; Budi Hartono, S.; Lu, G. Q. Monodisperse yolk-shell nanoparticles with a hierarchical porous structure for delivery vehicles and nanoreactors. *Angew. Chem., Int. Ed.* **2010**, *49*, 4981–4985.

[6] An, K.; Hyeon, T. Synthesis and biomedical applications of hollow nanostructures. *Nano Today* **2009**, *4*, 359–373.

[7] Cai, W. Q.; Yu, J. G.; Cheng, B.; Su, B.-L.; Jaroniec, M. Synthesis of boehmite hollow core/shell and hollow microspheres via sodium tartrate-mediated phase transformation and their enhanced adsorption performance in water treatment. *J. Phys. Chem. C* **2009**, *113*, 14739–14746.

[8] Wang, Z. Y.; Luan, D. Y.; Boey, F. Y. C.; Lou, X. W. Fast formation of SnO_2 nanoboxes with enhanced lithium storage capability. *J. Am. Chem. Soc.* **2011**, *133*, 4738–4741.

[9] Hong, Y. J.; Son, M. Y.; Kang, Y. C. One-pot facile synthesis of double-shelled SnO_2 yolk-shell-structured powders by continuous process as anode materials for Li-ion batteries. *Adv. Mater.* **2013**, *25*, 2279–2283.

[10] Lou, X. W.; Archer, L. A.; Yang, Z. C. Hollow micro-/nanostructures: Synthesis and applications. *Adv Mater.* **2008**, *20*, 3987–4019.

[11] Xu, S. M.; Hessel, C. M.; Ren, H.; Yu, R. B.; Jin, Q.; Yang, M.; Zhao, H. J.;Wang, D. α-Fe_2O_3 multi-shelled hollow microspheres for lithium ion battery anodes with superior capacity and charge retention. *Energy Environ. Sci.* **2014**, *7*, 632–637.

[12] Dong, Z. H.; Ren, H.; Hessel, C. M.; Wang, J. Y.; Yu, R. B.; Jin, Q.; Yang, M.; Hu, Z. D.; Chen, Y. F.; Tang, Z. Y. et al. Quintuple-shelled SnO_2 hollow microspheres with superior light scattering for high-performance dye-sensitized solar cells. *Adv. Mater.* **2014**, *26*, 905–909.

[13] Wang, Z. Y.; Zhou, L.; Lou, X. W. Metal oxide hollow nanostructures for lithium-ion batteries. *Adv. Mater.* **2012**, *24*, 1903–1911.

[14] Li, J. F.; Xiong, S. L.; Li, X. W.; Qian, Y. T. A facile route to synthesize multiporous $MnCo_2O_4$ and $CoMn_2O_4$ spinel quasi-hollow spheres with improved lithium storage properties. *Nanoscale* **2013**, *5*, 2045–2054.

[15] Qi, J.; Lai, X. Y.; Wang, J. Y.; Tang, H. J.; Ren, H.; Yu, Y.; Jin, Q.; Zhang, L. J.; Yu, R. B.; Ma, G. H. et al. Multi-shelled hollow micro-/nanostructures. *Chem. Soc. Rev.* **2015**, *44*, 6749–6773.

[16] Lu, A. H.; Li, W. C.; Hao, G. P.; Spliethoff, B.; Bongard, H. J.; Schaack, B. B.; Schuth, F. Easy synthesis of hollow polymer, carbon, and graphitized microspheres. *Angew. Chem., Int. Ed.* **2010**, *49*, 1615–1618.

[17] Xu, H. L.; Wang, W. Z. Template synthesis of multishelled Cu_2O hollow spheres with a single-crystalline shell wall. *Angew. Chem., Int. Ed.* **2007**, *46*, 1489–1492.

[18] Zeng, Y.; Wang, X.; Wang, H.; Dong, Y.; Ma, Y.; Yao, J. N. Multi-shelled titania hollow spheres fabricated by a hard template strategy: Enhanced photocatalytic activity. *Chem. Commun.* **2010**, *46*, 4312–4314.

[19] Chen, Y.; Chen, H. R.; Zeng, D. P.; Tian, Y. B.; Chen, F.; Feng, J. W.; Shi, J. L. Core/shell structured hollow mesoporous nanocapsules: A potential platform for simultaneous cell imaging and anticancer drug delivery. *ACS Nano* **2010**, *4*, 6001–6013.

[20] Dong, Z. H.; Lai, X. Y.; Halpert, J. E.; Yang, N. L.; Yi, L. X.; Zhai, J.; Wang, D.; Tang, Z. Y.; Jiang, L. Accurate control of multishelled ZnO hollow microspheres for dye-sensitized solar cells with high efficiency. *Adv. Mater.* **2012**, *24*, 1046–1049.

[21] Lai, X. Y.; Li, J.; Korgel, B. A.; Dong, Z. H.; Li, Z. M.; Su, F. B.; Du, J.; Wang, D. General synthesis and gas-sensing properties of multiple-shell metal oxide hollow microspheres. *Angew. Chem., Int. Ed.* **2011**, *123*, 2790–2793.

[22] Wang, J. Y.; Yang, N. L.; Tang, H. J.; Dong, Z. H.; Jin, Q.; Yang, M.; Kisailus, D.; Zhao, H. J.; Tang, Z. Y.; Wang, D. Accurate control of multishelled Co_3O_4 hollow microspheres as high-performance anode materials in lithium-ion batteries. *Angew. Chem., Int. Ed.* **2013**, *125*, 6545–6548.

[23] Qi, J.; Zhao, K.; Li, G. D.; Gao, Y.; Zhao, H. J.; Yu, R. B.; Tang, Z. Y. Multi-shelled CeO_2 hollow microspheres as superior photocatalysts for water oxidation. *Nanoscale* **2014**, *6*, 4072–4077.

[24] Xu, P. F.; Yu, R. B.; Ren, H.; Zong, L. B.; Chen, J.; Xing, X. R. Hierarchical nanoscale multi-shell Au/CeO_2 hollow spheres. *Chem. Sci.* **2014**, *5*, 4221–4226.

[25] Wang, Z.; Jia, W.; Jiang, M. L.; Chen, C.; Li, Y. D. One-step accurate synthesis of shell controllable $CoFe_2O_4$ hollow microspheres as high-performance electrode materials in supercapacitor. *Nano Res.* **2016**, *9*, 2026–2033.

[26] Zhang, Y. F.; Li, L. G.; Su, H. Q.; Huang, W.; Dong, X. C. Binary metal oxide: Advanced energy storage materials in supercapacitors. *J. Mater. Chem. A* **2015**, *3*, 43–59.

[27] Dong, X. C.; Xu, H.; Wang, X. W.; Huang, Y.-X.; Chan-Park, M. B.; Zhang, H.; Wang, L.-H.; Huang, W.; Chen, P. 3D graphene–cobalt oxide electrode for high-performance supercapacitor and enzymeless glucose detection. *ACS Nano* **2012**, *6*, 3206–3213.

[28] Sun, H. M.; Wang, L. M.; Chu, D. Q.; Ma, Z. C.; Wang, A. X. Facile fabrication of multishelled Cr_2O_3 hollow microspheres with enhanced gas sensitivity. *Mater. Lett.* **2015**, *140*, 158–161.

[29] Bai, F. H.; Xia, Y. D.; Chen, B. L.; Su, H. Q.; Zhu, Y. Q. Preparation and carbon dioxide uptake capacity of N-doped porous carbon materials derived from direct carbonization of zeolitic imidazolate framework. *Carbon* **2014**, *79*, 213–226.

[30] Qian, L.; Gu, L.; Yang, L.; Yuan, H. Y.; Xiao, D. Direct growth of $NiCo_2O_4$ nanostructures on conductive substrates with enhanced electrocatalytic activity and stability for methanol oxidation. *Nanoscale* **2013**, *5*, 7388–7396.

[31] Marco, J. F.; Gancedo, J. R.; Gracia, M.; Gautier, J. L.; Ríos, E. I.; Palmer, H. M.; Greaves, C.; Berry, F. J. Cation distribution and magnetic structure of the ferrimagnetic spinel $NiCo_2O_4$. *J. Mater. Chem.* **2001**, *11*, 3087–3093.

[32] Marco, J. F.; Gancedo, J. R.; Gracia, M.; Gautier, J. L.; Ríos, E.; Berry, F. J. Characterization of the nickel cobaltite, $NiCo_2O_4$, prepared by several methods: An XRD, XANES, EXAFS, and XPS study. *J. Solid State Chem.* **2000**, *153*, 74–81.

[33] Jiménez, V. M.; Fernández, A.; Espinós, J. P.; González-Elipe, A. R. The state of the oxygen at the surface of polycrystalline cobalt oxide. *J. Electron Spectrosc. Relat. Phenom.* **1995**, *71*, 61–71.

[34] Choudhury, T.; Saied, S. O.; Sullivan, J. L.; Abbot, A. M. Reduction of oxides of iron, cobalt, titanium and niobium by low-energy ion bombardment. *J. Phys. D: Appl. Phys.* **1989**, *22*, 1185–1195.

[35] Liu, X. Y.; Shi, S. J.; Xiong, Q. Q.; Li, L.; Zhang, Y. J.; Tang, H.; Gu, C. D.; Wang, X. L.; Tu, J. P. Hierarchical $NiCo_2O_4$@$NiCo_2O_4$ core/shell nanoflake arrays as high-performance supercapacitor materials. *ACS Appl. Mater. Interfaces* **2013**, *5*, 8790–8795.

[36] Guo, D.; Zhang, H. M.; Yu, X. Z.; Zhang, M.; Zhang, P.; Li, Q. H.; Wang, T. H. Facile synthesis and excellent electrochemical properties of $CoMoO_4$ nanoplate arrays as supercapacitors. *J. Mater. Chem. A* **2013**, *1*, 7247–7254.